Design of an Active Controlled Caster Aiming at Cart with Low Crashes/Vibrations

Kiyoshi IOI*1, Atsushi SUDA*2 and Masahiko YAMAMOTO*3

*1 Faculty of Science and Engineering, Kinki University
3-4-1, Kowakae, Higashi-osaka, Osaka, 577-8502, JAPAN
ioi@mech.kindai.ac.jp

*2, 3 Yuei Caster co.ltd.
1-8-39, Honjyo-nishi, Higashi-osaka, Osaka, 578-0965, JAPAN
a.suda@yueicaster.co.jp, yamamas2000@yahoo.co.jp

Abstract

This paper presents experimental and simulational results of a cart with an active controlled caster to reduce the cart crashes and vibrations. First the active controlled caster is introduced, which has a mechanical low-crash structure based on the idea of center of percussion. Next the dynamical model of the cart with the caster is derived to study the caster control for the low crashes and vibrations. Then we show experimental results of the cart with the caster controlled by the acceleration and velocity signals, compared to the simulation results. The proposed control is verified to effectively reduce the impulsive crashes and vibrations of the cart.

Keywords: caster, design, control, dynamics

1 Introduction

In recent years, it has been eagerly desirable that patients, medicines and small precision parts should be carried smoothly and quietly by advanced carts with casters. In order to realize the ideal cart with low crashes and vibrations, some casters equipped with damping elements have been developed [1]. On the other hand, although the casters with dampers can restrict the cart vibrations, they had little ability to reduce the crashed acceleration of the cart. Hence we designed a new caster focusing on the center of percussion of the caster, and verified experimentally the effective reduction of the cart accelerations using a cart with the new caster [2], [3]. However, the cart vibrations were not removed effectively by the new caster.

Thus we design an active controlled caster that has a mechanical low-crashed structure based on the idea of center of percussion. First the dynamical model of the cart with a caster is derived to study the control method for low crashes and vibrations. Next we show experimental results of the cart with the caster controlled by the acceleration and velocity signals, compared to the simulation results. The application of the control design is verified to effectively reduce the impulsive crashes and vibrations of the cart. Finally we in brief discuss the effect of the disturbance control using the transfer functions and Bode gain diagrams of the cart model.

2 Active caster with low-crash mechanism

2.1 Low-crash mechanism of caster

Figure 1 shows a side view of a swing-arm typed caster with an elastic and viscous element. The elastic and viscous element has usually effects to reduce the cart vibrations, and also has a role to keep the swing arm horizontal. On the other hand, the cart has large crushes through the swing arm when the caster wheel with the swing arm collides with a small bump on a road. It is rather difficult for the momentary crashes to be removed by only the elastic and viscous element. Thus we have proposed a mechanical design based on the center of percussion of the swing arm with a wheel. We summarize the design concept as follows.

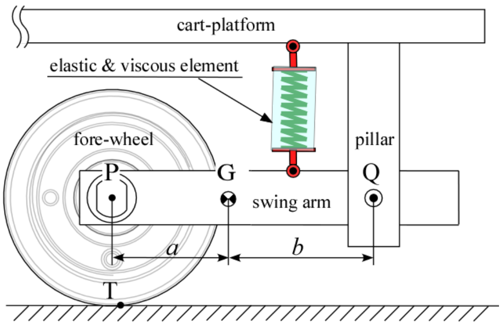

Fig. 1 Side view of swing-arm typed caster

The impulsive force from a road to the wheel center P is nearly perpendicular to the line PQ shown in Figure 1 when the caster wheel collides with a small bump. Hence the transmitted impulsive force to the joint center Q is expected to be effectively reduced when the point Q is located on the center of percussion of the whole swing arm against the point P. The design condition is as follows:

$$mab = I_G . \tag{1}$$

Here Symbols a and b denote the length between the point P and the gravity center G of the swing arm, and the length between the point G and the point Q, respectively. Symbols m and I_G denote the mass of the swing arm and the moment of inertia about the gravity center G, respectively. Appling the above concept based on Equation (1) to the swing arm design, we have verified experimentally the effective reduction of the crashes against the cart [2], [3]. However, the residual vibrations of the cart were not removed effectively even by the new designed caster.

2.2 Design of active caster

Here, an active controlled caster is proposed, which has the design concept based on center of percussion introduced in the above section. The support spring is also located to keep the swing arm horizontal between the swing arm and the cart-platform in **Figure 2**, as shown in Figure 1. A voice coil motor (VCM) is newly set up as a prismatic actuator on behalf of the fixed pillar in Figure 1. It is likely to enlarge the actuator's size when only the VCM supports both the inertial force and the cart weight, and thus two springs are placed parallel to the VCM to compensate the cart weight. Two linear bushes are also equipped to make the movement of the VCM smooth. The side and front views are shown in **Figure 2**.

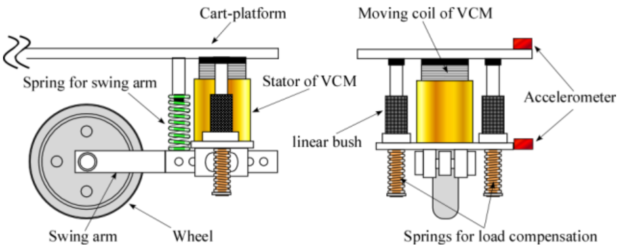

Fig. 2 Side and front views of active caster

3 Modeling of cart with active caster

3.1 Motion equation of cart with active caster

Here, we formulate the two-dimensional motion equation of a cart with the active caster. The angle and mass of the cart-platform are assumed to be negligibly small, and to concentrate at one point on the platform, respectively. The caster wheel has also an elastic and viscous property that transmits an external force f_e from a road when the wheel contacts the road at Point T on itself. **Figure 3** shows the side view of the cart, which has a bearing support, a spring for the swing arm and a spring for the cart-load compensation. Points Q and A denote the rotational center of the swing arm and the attached point of the spring for the swing arm, respectively.

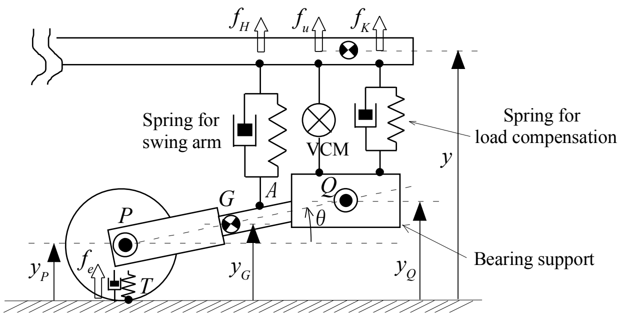

Fig. 3 Side view model of cart with active caster

Here we define Symbols in Figure 3 as follows:

y: Height from a road to the reference point of the cart,
y_P: Height from a road to the wheel center P,
y_Q: Height from a road to the swing arm center Q,
y_G: Height from a road to the mass center G of the swing arm,
θ: Swing arm angle from the horizontal road,
M: Equivalent mass of the cart at the reference point,
m_Q: Mass of the bearing support,
m: Mass of the swing arm with the wheel,
f_u: Operational force of the VCM to the cart,
f_K: Passive force of the load spring to the cart,
f_H: Passive force of the swing arm's spring to the cart,
f_e: External force from the road to the caster wheel,
f_Q: Constraint force to the bearing support at Point Q.

In addition to the above modeling parameters, the distance between Point G and Point A is defined as Symbol e, and Symbols a and b are also defined as shown in Figure 1. **Figure 4** in particular shows the distance parameters about the swing arm.

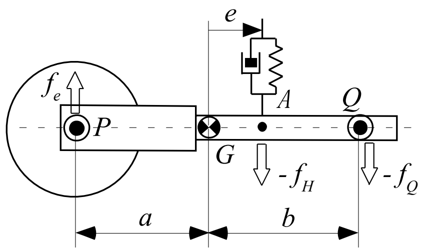

Fig. 4 Distance parameters about swing arm

We derive the motion equation when the angle of the cart-platform from the road is small enough.

Assuming that the external force f_e itself becomes the transmitted force at the wheel center P, we obtain the vertical Newton's Equations of the cart with the active caster as follows:

$$M\ddot{y} = f_u + f_K + f_H - Mg \text{ ,} \tag{2}$$

$$m_Q\ddot{y}_Q = -f_u - f_K + f_Q - m_Q g \text{ ,} \tag{3}$$

$$m\ddot{y}_G = -f_Q - f_H + f_e - mg \text{ .} \tag{4}$$

Considering that the swing arm rotates, we also obtain the following Euler's Equation:

$$I_G\ddot{\theta} = -af_e - ef_H - bf_Q \text{ .} \tag{5}$$

Here Symbol I_G denotes the moment of inertia about Point G. The swing arm angle θ is also neglected in the right terms of Equation (5) under the approximate conditions $\cos\theta \cong 1$ and $\sin\theta \cong 0$.

On the other hand, the heights y, y_G and the angle θ have the following geometrical relationship:

$$\begin{aligned} y_G &= y_Q + b\sin\theta \\ &\cong y_Q + b\theta \cdot \end{aligned} \tag{6}$$

Substituting Equation (6) into Equation (5), and eliminating the angle θ and the constraint force f_Q, we obtain the following formulations:

$$m\ddot{y}_G + m_Q\ddot{y}_Q = -f_u - f_K - f_H + f_e - (m + m_Q)g \text{,} \tag{7}$$

$$\left(m+\frac{I_G}{b^2}\right)\ddot{y}_G-\frac{I_G}{b^2}\ddot{y}_Q=\left(1+\frac{a}{b}\right)f_e-\left(1-\frac{e}{b}\right)f_H-mg\,. \quad (8)$$

For the reduction of design variables, we define new variables as follows:

$$\frac{I_G}{b^2}\equiv m_G,\ \ \frac{a}{b}\equiv\mu,\ \ \frac{e}{b}\equiv\lambda\,.$$

Here Symbol m_G is considered to denote the equivalent mass of the swing arm about Point Q. Substituting new variables into Equation (8), we obtain the following new expression:

$$\left(m+m_G\right)\ddot{y}_G-m_G\ddot{y}_Q=\left(1+\mu\right)f_e-\left(1-\lambda\right)f_H-mg\,. \quad (9)$$

Equations (2), (7) and (9) are the final motion equations of the cart with the active caster.

3.2 Modeling of elastic and viscous force

The passive forces f_K and f_H are formulated as linearly elastic and viscous elements as follows:

$$f_K=K_S\left\{l_{S0}-\left(y-y_Q\right)\right\}-C_S\left(\dot{y}-\dot{y}_Q\right), \quad (10)$$

$$f_H=K_H\left\{l_{H0}-\left(y-y_A\right)\right\}-C_H\left(\dot{y}-\dot{y}_A\right). \quad (11)$$

Here Symbols K_S, C_S and l_{S0} denote the spring constant, the viscous coefficient and the natural length of the load spring, respectively. Similarly Symbols K_H, C_H and l_{H0} denote the spring constant, the viscous coefficient and the natural length of the swing arm spring, respectively.

Since Symbol y_A means the height of Point A from the road, the following relationship is obtained geometrically:

$$y_A\cong\left(1-\frac{e}{b}\right)y_G+\frac{e}{b}y_Q=\left(1-\lambda\right)y_G+\lambda y_Q\,. \quad (12)$$

Next we describe the external force to the caster wheel from the road. The external force f_e is also formulated as an elastic and viscous element similar to above passive spring/dampers when the caster wheel runs on a flat road as shown in **Figure 5**. The formulation is as follows:

$$f_e=K_T(R-y_P)-C_T\dot{y}_P\,. \quad (13)$$

Here Symbols K_T, C_T and R denote the spring constant, the viscous coefficient and the natural radius of the wheel tire, respectively. On the other hand, the vertically external force f_e is formulated as follows when the caster wheel collides with a hard and small bump:

$$f_e=\left(K_T\Delta Z+C_T\Delta\dot{Z}\right)\frac{y_P}{\sqrt{\left(a-x_P\right)^2+y_P{}^2}}\,. \quad (14)$$

Here Symbols ΔZ and $\Delta\dot{Z}$ denote the lapping displacement between the wheel circle and the semicircular bump, and the velocity of that displacement, respectively. In this case, Symbols ΔZ and $\Delta\dot{Z}$ are expressed as follows as shown in **Figure 6**:

$$\Delta Z=(R+r)-\sqrt{(a-x_P)^2+y_P{}^2}$$

$$\Delta\dot{Z}=\frac{1}{\sqrt{(a-x_P)^2+y_P{}^2}}\left\{\left(a-x_P\right)\dot{x}_P-y_P\dot{y}_P\right\}\,. \quad (15)$$

Here Symbols a and r denote the center position and the radius of a semicircular bump, respectively.

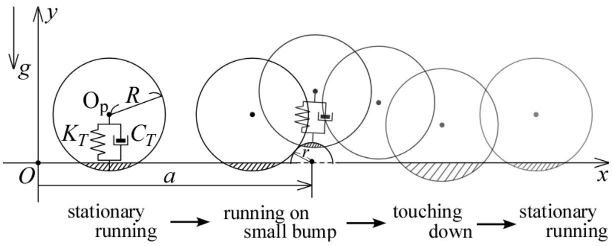

Fig. 5 Motion appearance of caster wheel

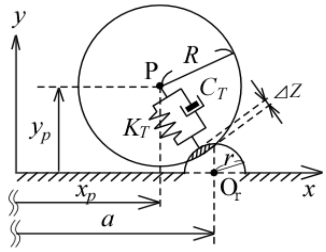

Fig. 6 Contact with a semicircular bump

The selection of Equation (13) or Equation (14) is determined by the arithmetic sign of ΔZ. Additionally the velocity of the wheel center is substituted for that of the cart, and the position of the wheel center x_p is obtained by time integral of the velocity.

3.3 Modeling of VCM and control design

The VCM is simply formulated as a linear actuator with well-known DC motor properties:

$$v_i=L\frac{di}{dt}+Ri+v_e,\ \ v_e=K_e\dot{x},\ \ f_u=K_f i\,. \quad (16)$$

Here Symbols v_i, v_e and i denote the input voltage, the induction voltage and the electrical current, respectively. Symbols L, R, K_e and K_f denote the inductance, the resistance, the inductive constant and the force constant, respectively. In addition to the above motor's properties, the amplifier's property driving the VCM is assumed as a transfer function with one-order lag system as follows:

$$G_A(s)=\frac{A_m}{1+Ts}\,. \quad (17)$$

Here Symbols A_m and T denote the direct current gain and the time constant of the amplifier, respectively.

Combining motion Equations (2), (7) and (9) with Equations (10) – (17), we obtain the whole cart model including an active caster equipped with a VCM.

Next we describe the control design for low crashes and vibrations of the cart. What is called, sky-hook damper has been well known to reduce the vibrations of cars in the automobile engineering. However, the caster wheel is different from the conventional car wheel because the center of the caster wheel has a lever offset from the vertically rotational axis of the caster. Hence two accelerometers are placed on both the cart-platform and the rotational center Q of the swing arm as shown in **Figure 2**. Two accelerations of $\ddot{y}$ and $\ddot{y}_Q$ are acquired by using these two accelerometers. Since the acceleration signals generally have many noises at high frequencies, appropriate low pass filters are added to remove these noises. After applying the low pass filters to the acceleration signals, the velocities are also acquired by time integral of the signals. The whole feedback signals are obtained by the combination of accelerations and velocities. **Figure 7** shows the controller of the cart with an active caster.

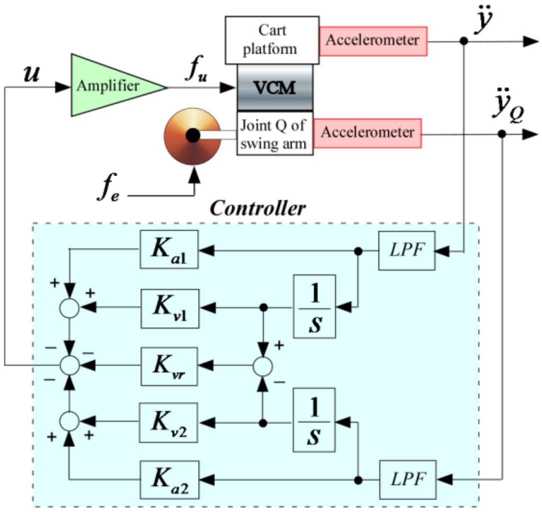

Fig. 7 Controller for low crash and vibration

4 Experiment of cart with active caster

4.1 Hardware system

First, the hardware components are shown. **Figure 8** and **Table 1** show the VCM (voice coil motor) for control and the electrical specifications, respectively.

a) Stator b) Moving coil

Fig. 8 Components of VCM

Table 1 Electrical specifications of VCM

	symbol	value
Resistance [Ω]	R	5.2
Inductance [H]	L	6.42×10^{-3}
Force constant [N/A]	Kf	15.5
Back-emf constant [V/(m/s)]	Ke	15.5
Direct current gain [V/V]	Am	4.6
Time constant [msec]	T	20

Table 2 Mechanical specifications of swing arm

	symbol	value
Distance of point P and point G [m]	a	0.029
Distance of point G and point Q [m]	b	0.098
Mass of swing arm [kg]	m	0.816
Moment of inertia about point G [kgm2]	I_G	2.62×10^{-3}

The swing arm is designed as a specific arm based on the idea of center of percussion as mentioned in Chapter 2. **Table 2** shows the mechanical specifications of the swing arm. **Table 3** shows each mass of the cart with the swing arm. **Table 4** shows the specific parameters of spring components. **Table 5** shows the parameters of the wheel tire that were measured by experiments.

Table 3 Masses of main parts

	symbol	value
Mass of support [kg]	m_Q	1.39
Virtual mass of swing arm [kg]	m_G	0.27
Virtual mass of cart [kg]	M	1.23

Table 4 Specific parameters of spring components

	symbol	value
Natural length of spring for load compensation [m]	l_{S0}	9.85×10^{-2}
Spring constant for load compensation[N/m]	K_S	4.00×10^{3}
Viscous coefficient [N/(m/s)]	C_S	4
Natural length of spring for swing arm [m]	l_{H0}	1.17×10^{-1}
Spring constant for swing arm[N/m]	K_H	3.91×10^{4}
Viscous coefficient [N/(m/s)]	C_H	8

Table 5 Parameters of wheel tire

	symbol	value
Radius [m]	r	0.05
Spring constant [N/m]	K_t	1.20×10^{5}
Viscous coefficient [N/(m/s)]	C_t	200

Figure 9 shows the experimental setup for the cart with the active caster. The cart is pushed out at 1100[mm/sec] by a linear servo system, and runs on an aluminum plate. A semicircular bump is placed on the plate, which has a radius of 2.5[mm]. All of motion data are acquired by a personal computer. The feedback control is conducted using Labview^{TM} real-time system.

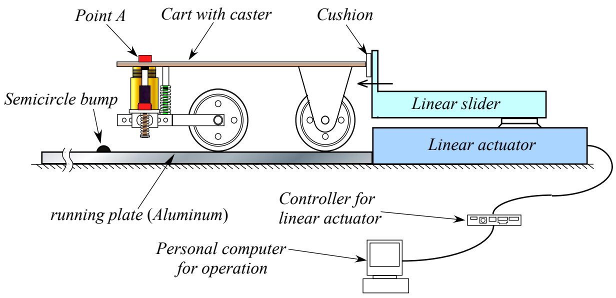

Fig. 9 Experimental setup for cart with active caster

4.2 Experimental result

In this section, we confirm the effects of the active control by experimental results, compared to simulation results. All of the experiments and simulational are conducted under the condition as shown in **Figure 9**.

Figure 10 shows the acceleration response of Point A on the cart platform in **Figure 9** when the caster runs and collides with a small bump without control. The experiment has a good agreement with the simulation from the viewpoint of resonant frequency, and the convergent time to zero is a little different between the experiment and the simulation.

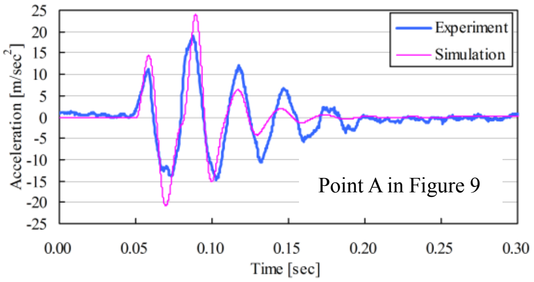

Fig. 10 Acceleration response without control

Next we show some results with feedback control. These experiments and simulations have the low pass filters of 130 [Hz] to remove sensory noises and the cycle time of 1 [msec] to realize real-time control.

Figure 11 shows the controlled result with the feedback signal of only relative velocity. This feedback effect is considered to correspond to the mechanical damping effect between the cart and the bearing support. The residual vibrations are largely repressed, and the first impulsive acceleration is not reduced, compared to that in **Figure 10**.

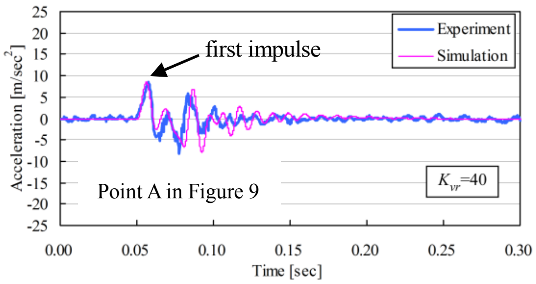

Fig. 11 Acceleration response with control

Figure 12 shows the control result with the feedback signals of relative velocity and cart acceleration. The first impulsive acceleration is rather reduced by virtue of the feedback signal of cart acceleration. The acceleration feedback is considered to change the equivalent mass of the cart virtually. **Figure 12** reveals that the vibrational components with high frequencies increase compared to **Figure 11**.

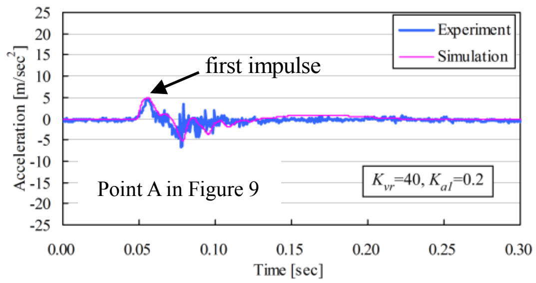

Fig. 12 Acceleration response with control

Figure 13 shows the control result with the additional feedback signal of the velocity of bearing support in order to remove the above vibrations with high frequencies. The simulation results in **Figure 13** have better agreements with experimental results than those in **Figure 10**, because the uncertain elements such as frictions and backlashes are considered to be largely restricted by feedback control.

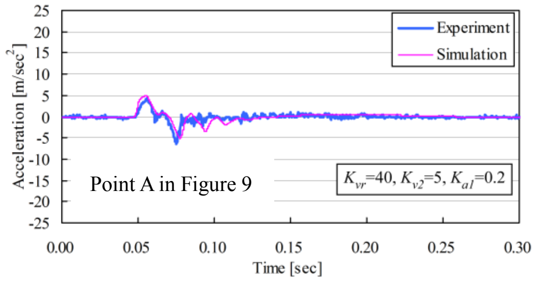

Fig. 13 Acceleration response with control

Comparing **Figure 10** to **Figure 13**, we confirm that the maximum value of the cart acceleration becomes about 1/4 and the damping time of the residual vibration becomes about 1/5 by virtue of feedback control.

4.3 Discussion of control performance

In this section, we discuss the control performance by using the transfer function and Bode diagram of the objective model. First, adding Equation (2) to Equation (7), we obtain the following relationship:

$$m\ddot{y}_G + m_Q\ddot{y}_Q + M\ddot{y} = f_e - (m + m_Q + M)g. \tag{18}$$

Applying Equations (7), (9) and (18), the transfer function of the objective model is derived. The following modified variables are newly defined to set the equilibrium points at initial points with zero values:

$$F_e \equiv f_e - f_{e0},\ F_H \equiv f_H - f_{H0},\ F_u \equiv f_u - f_{u0},$$
$$F_K \equiv f_K - f_{K0},\ Y \equiv y - y_0,\ Y_Q \equiv y_Q - y_{Q0},\ Y_G \equiv y_G - y_{G0}.$$

Applying *Laplace* transformation to Equations (7), (9) and (18), we obtain the following matrix form:

$$\begin{bmatrix} (m+m_G)s^2 & -m_G s^2 & 0 \\ ms^2 & m_Q s^2 & 0 \\ ms^2 & m_Q s^2 & Ms^2 \end{bmatrix} \begin{bmatrix} Y_G \\ Y_Q \\ Y \end{bmatrix}$$
$$= \begin{bmatrix} (1+\mu)F_e + (1-\lambda)G_H\{Y-(1-\lambda)Y_G - \lambda Y_Q\} \\ -F_u + F_e + G_s(Y - Y_Q) + G_H\{Y-(1-\lambda)Y_G - \lambda Y_Q\} \\ F_e \end{bmatrix}, \tag{19}$$

where $sC_s + K_s \equiv G_s(s)$, $sC_H + K_H \equiv G_H(s)$.

The output $s^2Y(s)$ is represented by both the operational input $F_u(s)$ and the external force $F_e(s)$ from Equation (19), as follows:

$$s^2Y(s) = \frac{\left(a_2(s)s^2 + a_0(s)\right)F_e(s) + s^2\left(C_2 s^2 + C_0(s)\right)F_u(s)}{b_4 s^4 + b_2(s)s^2 + b_0(s)}. \tag{20}$$

Here, new symbols are defined as follows.

$$a_2(s) \equiv \{m_G - \mu\lambda m + (1+\mu)(1-\lambda)m_Q\}G_H(s)$$
$$+ (m_G - \mu m)G_s(s),$$
$$a_0(s) \equiv (1-\lambda)^2 G_s(s)G_H(s),$$
$$b_4(s) = b_4 \equiv M(mm_G + m_G m_Q + m_Q m),$$

$$b_2(s) \equiv M\left\{(m+m_G)G_s(s)+\left(\lambda^2 m+m_G+(1-\lambda)^2 m_Q\right)G_H(s)\right\}$$
$$+\left(mm_G+m_G m_Q+m_Q m\right)\left(G_s(s)+G_H(s)\right),$$
$$b_0(s) \equiv (1-\lambda)^2\left(M+m_Q+m\right)G_s(s)G_H(s),$$
$$C_2(s)=C_2 \equiv mm_G+m_G m_Q+m_Q m,$$
$$C_0(s) \equiv (1-\lambda)\left\{(1-\lambda)m_Q-\lambda m\right\}G_H(s).$$

Here we represent the Bode gain diagram from the disturbance input f_e to the acceleration output $\ddot{y}$, based on Equation (20). It is noticed that the operational input $F_u(s)$ includes the properties of the actuator and LPF as shown in **Figure 7**.

The green curves and blue curves in **Figure 14** show the result with the feedback signal of only relative velocity and that without control, respectively. The assumed condition of the Bode gain diagram with control corresponds to that of the acceleration response shown in **Figure 11**. We can see that the two resonant frequencies of 4[Hz] and 35[Hz] transfer to those of 13[Hz] and 100[Hz] by virtue of feedback control. Although the amplitude of the past resonant frequency of 35[Hs] is largely reduced, that about the new frequency of 100[Hz] rather increases. The tendency of amplitudes that appeared in **Figure 14** is also confirmed to be similar to that in **Figure 11**.

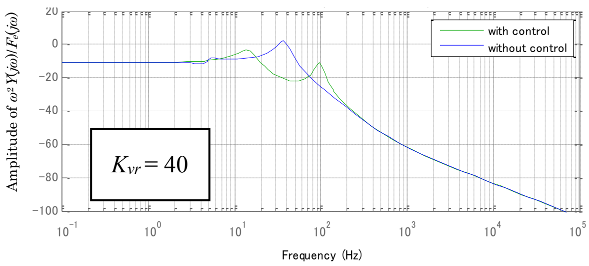

Fig. 14 Bode gain diagram-1

Figure 15 shows the case with the additional feedback signals of the cart acceleration and the velocity of bearing. The blue curve in **Figure 15** is same as that in **Figure 14**. The assumed condition of the Bode gain diagram with control corresponds to that of the acceleration response shown in **Figure 13**. We can confirm that the amplitude of the resonant frequency of 100[Hz] becomes smaller and flatter than that shown in **Figure 14**, and consequently the residual vibration of the cart rapidly converges to zero as shown in **Figure 13**.

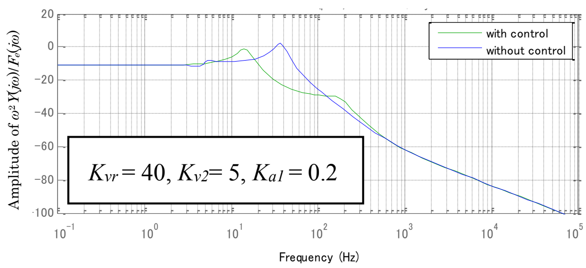

Fig. 15 Bode gain diagram-2

5 Conclusion

This paper reported an active controlled caster to reduce the cart crashes and vibrations. The main results are as follows:

1) The active controlled caster was proposed, which was designed under the concept of center of percussion.
2) The dynamical model of the cart with an active caster was derived including the actuator dynamics to study impulsive accelerations and control design.
3) The experimental results had good agreements with the simulation results calculated using the dynamical model.
4) The cart acceleration became about 1/4 and the damping time of the residual vibration became about 1/5 by virtue of feedback control.
5) The control performances were discussed using the Bode gain diagram of the dynamical model.

In this study, the distribution and combination of feedback gains were determined by trials and errors, according to the observation of the actual responses. The systematic determination of gains is left in future works. It is also important for the dynamical model of the cart to be improved to be applicable to not only the vertical motion but also the horizontal motion.

The MEXT-supported program for the strategic Research Foundation at Private Universities (2012-2014) is acknowledged.

References

[1] A.Suda, K.Ioi and M.Yamamoto, “Elasticity Estimation and Property Measurement of Urethane Damper with Embedded Spring”, Journal of JSDE, Vol. 47, No. 6, (2012), pp.294-299.
[2] K.Ioi, T.Kawabuchi, A.Suda, and K.Moriya, “Mechanical and Control Design of Caster for Low Vibrations and Crashes of Carts”, Proc. of IEEE ICMA, (2011), pp.1688-1693.
[3] A.Suda, K.Moriya, K.Ioi and M.Yamamoto, “Study on a Wheeled Caster for Design of Low-Crash Wagons”, Journal of JSME, Vol.77, No.777, (2011), pp.1998-2007.
[4]A.Suda, K.Ioi, N.Tsujino, S.Iguchi and M.Yamamoto, “Development of Active Caster to Achieve Low Vibration/Impact Cart”, USB Proc. of JSME D&D, (2013), No.327.
[5] JSME, “Front Lines of Motion and Vbration Control”, Kyoritsu Press, (2007).
[6]K.Nonami, “Vibration Control and System Dynamics ”, Corona Press, (2010).

Received on October 25, 2013
Accepted on January 22, 2014